www.springer.com/41230
https://doi.org/10.1007/s41230-026-5239-6

Effect of casting and heat treatment parameters on microstructure and tensile properties of a nickel-based polycrystalline superalloy at 1000 °C

***Gao-yang Jing[1, 2], Hai-tao Jiang[1, 2], Yu-quan Hao[1, 3], Tian-yu Liu[1, 2], Lei Jin[1, 2], Guo-yan Shui[1, 2], Lan-bo Ma[1, 2], Yi-peng Li[1, 2], Yang Guan[1, 2], and Yi-zhong Jiang[1, 2]**

1. Shenyang Research Institute of Foundry Co., Ltd. CAM, Shenyang 110022, China

2. State Key Laboratory of Advanced Casting Technologies, Shenyang 110022, China

3. Test Institute for Moulding Materials & Castings for Mechanical Industry (Shenyang) Limited Company, Shenyang 110022, China

Copyright © 2026 Foundry Journal Agency

Abstract: The effects of pouring temperature, shell mold temperature, and heat treatment parameters on the microstructure and high-temperature tensile properties of a γ' phase strengthened nickel-based superalloys were systematically investigated. Metallographic analysis, SEM observation, and high-temperature tensile testing results indicate that lower pouring and shell mold temperatures effectively reduce the grain size and MC carbide dimensions, refine the as-cast primary γ' phase, thereby decrease the size of residual primary γ' phase after heat treatment. The cooling method following solution heat treatment was identified as a key process parameter affecting high-temperature mechanical properties. Under air-cooling conditions, the alloy exhibits a higher tensile strength of 532.00±10.24 MPa, but relatively low ductility, with an elongation of (4.00±1.08)%. By contrast, furnace cooling significantly improves high-temperature ductility, yielding a maximum elongation of (11.75±0.35)%, but reducing the strength to 477.5±7.79 MPa. Experimental results confirm a clear correlation between γ' phase size and mechanical properties: as γ' phase size increases, the alloy strength gradually decreases while elongation increases. The high-temperature tensile fracture is predominantly intergranular, with cracks initially forming around MC carbides and subsequently propagating along grain boundaries. The research findings provide important guidance for industrial production process optimization of this alloy and offer significant insights into process parameter selection for balancing strength and ductility.

Keywords: process parameters; nickel-based superalloy; microstructure; mechanical properties; cooling method

CLC numbers: TG146.1+5 **Document code:** A **Article ID:** 1672-6421(2026)06-827-11

1 Introduction

With the continuous advancement of aviation technology, the thrust-to-weight ratio and combustion chamber operating temperature of aircraft engines are constantly increasing, requiring engine components to possess high reliability and durability to withstand increasingly complex service environments[1-3]. Nickel-based polycrystalline superalloys strengthened by γ' phase precipitation are extensively used in the production of aero-engine components due to their high strength and structural stability, excellent high-temperature resistance, and comparatively low manufacturing costs[4-6]. The mechanical properties of superalloys are key performance indicators for the reliability and operational durability of engine components. These properties primarily depend on the material's microstructural characteristics, which are comprehensively influenced by the thermal history of liquid metal, solidification processes, and subsequent heat treatment. These process parameters ultimately tailor the mechanical performance through microstructure refinement, reduced elemental segregation, and enhanced precipitation of strengthening phase[2, 7-9]. Research on superalloys has predominantly focused on microstructural

***Gao-yang Jing**

Male, born in 1990, Master, Engineer. His research interests primarily focus on composition design, melting, and property control of cast superalloys.

E-mail: jgysteel@163.com

Received: 2025-10-05; Revised: 2026-01-20; Accepted: 2026-01-27

evolution and mechanical-property regulation across different compositional systems, with particular emphasis on strength and creep life[6, 10-12], because at high temperatures the service limit is primarily governed by creep deformation/rupture, which is directly controlled by key strengthening mechanisms. In fact, ductility not only determines the processing performance of the alloy, but is also a critical parameter in high-temperature service environments[13].

Since strength and ductility typically exhibit an inverse relationship, excessive pursuit of strength often sacrifices ductility, increasing the risk of inadequate performance. Therefore, rational design of process routes is essential to achieve excellent strength while maintaining sufficient ductility for application requirements. This study investigated a γ' phase-strengthened nickel-based polycrystalline superalloy for high-temperature thin-walled structures and turbine components of aircraft engines. The effects of pouring temperature, mold temperature, and heat treatment parameters on its microstructure and tensile properties at 1,000 °C were systematically investigated. The findings are expected to provide important guidance for the optimization of industrial production.

2 Materials and experiment

The nominal chemical compositions (mass%) of the superalloy used in this study were: 9.6Cr, 13.5Co, 0.8Nb, 8.9Mo, 1.4W, 4.45Ti, 5.58Al, 0.17C, with Ni as balance. During the experiment, a 5 kg ingot was placed in an alumina crucible within a 25 kg vacuum induction melting furnace. After reducing the chamber pressure below 0.1 Pa, the power was gradually increased until the melt temperature reached 1,550 °C and maintained for 5 min to ensure homogeneity of composition and temperature in the molten pool. Subsequently, the melt was rapidly cooled to the predetermined pouring temperature and poured within 3 s into alumina ceramic molds that had been preheated at various temperatures for 360 min and embedded in sand. The detail casting parameters are listed in Table 1. The shell mold morphology and geometric dimensions of the test bars are detailed in Ref. [14].

After sand blasting and cutting, the test bars were placed in vacuum glass tubes for solution heat treatment (1,210 °C, 240 min) and aging treatment. Two cooling methods were employed for the solution heat treatment: air cooling and furnace cooling (with the furnace door open). By contrast, only air cooling was used following the aging treatment. Table 1 lists the sample designations and corresponding experimental parameters. High-temperature tensile tests were conducted at 1,000 °C according to the Standard GB/T228.2-2015, with two test bars tested for each set of parameters.

Transverse samples were sectioned from the test bars for metallographic analysis. After grinding and polishing, the samples were chemically etched using a mixed solution of 1.5 g copper sulfate, 40 mL hydrochloric acid, and 20 mL ethanol, and then examined using a stereomicroscope and an optical microscope (ZEISS Axio Vert. A1) to observe the microstructure. The polished samples were subsequently subjected to electrolytic etching in a mixed solution of 84 mL phosphoric acid, 68 mL sulfuric acid, and 48 mL water, etched for 3–5 s at 5 V to remove the γ phase. A scanning electron microscope (SEM, EVO MA25) was employed to observe the γ/γ' phases and tensile fracture surfaces, while energy-dispersive X-ray spectroscopy (EDS, extra high tension, EHT=20 kV; working distance, WD=10.5 mm) was used for semi-quantitative analysis of the microstructural composition. For each sample, the sizes of grains, MC carbides, and γ' precipitates were measured on 5 micrographs following standard metallographic methods.

Table 1: Experimental parameters employed in this study

Sample No.	Pouring		Solution heat treatment			Aging treatment		
	Pouring temp. (°C)	Shell mold temp. (°C)	Temp. (°C)	Time (min)	Cooling	Temp. (°C)	Time (min)	Cooling
1	1,520	900	1,210	240	Air cooling	–	–	
2	1,480	900	1,210	240	Air cooling	–	–	
3	1,480	700	1,210	240	Air cooling	–	–	
4	1,480	900	1,210	240	Furnace cooling	–	–	
5	1,480	900	1,210	240	Furnace cooling	1,100	120	Air cooling

3 Results

3.1 Microstructure and chemical composition of precipitated phases

Since the chemical compositions of precipitated phases under various experimental conditions were essentially consistent, Sample 1 was used as an example to illustrate the compositional characteristics of each precipitated phase. Figure 1 shows the microstructure of the alloy as-cast and after solution treated. Table 2 presents the specific EDS analysis results, with the corresponding detection positions marked in Fig. 1. It can be found that MC carbides are primarily enriched

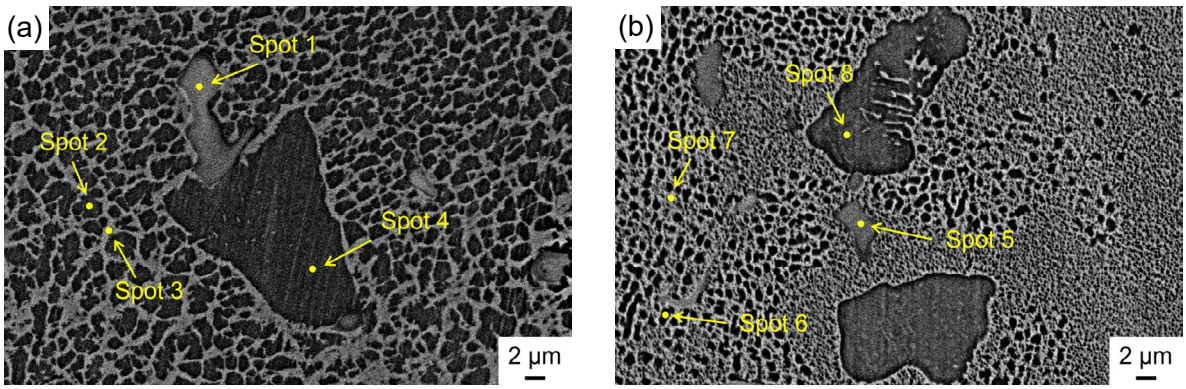


Fig. 1: Microstructure of superalloy in as-cast (a) and solution-treated (b) conditions (Sample 1)

Table 2: EDS analysis results of precipitates in Sample 1 (wt.%)

State	Location	Phases	C	Al	Ti	Cr	Co	Ni	Nb	Mo	W
As-cast	Spot 1	MC	8.28	0.03	41.92	1.65	0.51	2.35	20.06	16.64	8.54
	Spot 2	γ'	2.60	3.81	6.00	5.66	11.32	65.33	0.59	1.41	3.28
	Spot 3	γ	2.58	3.34	5.24	7.29	12.44	63.28	0.44	1.93	3.46
	Spot 4	(γ+γ') eutectics	2.70	3.79	7.56	3.89	10.67	67.61	0.51	1.00	2.27
Heat treatment	Spot 5	MC	8.54	0.08	41.90	1.34	0.52	2.60	25.21	14.90	4.92
	Spot 6	γ'	3.17	3.42	5.82	6.28	11.59	65.62	0.41	1.03	2.52
	Spot 7	γ	2.57	2.71	3.71	13.16	15.85	54.33	0.49	3.37	3.82
	Spot 8	(γ+γ') eutectics	2.94	3.78	7.20	4.05	10.36	66.24	0.67	1.09	3.67

with Nb and Mo elements. After heat treatment, the Nb content significantly increases, while the Mo and W contents decrease, indicating that heat treatment promotes the redistribution of elements in MC carbides. The γ' phase is rich in Ni, Al, and Ti elements, with minimal compositional changes before and after heat treatment. In the γ matrix, the Ni content decreases significantly after heat treatment, while Cr and Co contents increase markedly, suggesting that solution heat treatment facilitates the redistribution of Cr and Co elements. For the (γ+γ') eutectic structure, except for a slight increase in W content, the distribution of other elements remaines essentially stable, demonstrating that heat treatment has limited impact on the composition of eutectic structures.

3.2 Microstructure evolution under different processes

3.2.1 Grain size

As shown in Fig. 2, the alloy exhibits equiaxed grain structures under various processing conditions. The grain size is primarily influenced by casting process parameters, decreasing significantly with the decrease of pouring temperature and mold temperature. Sample 1 (pouring temperature 1,520 °C, mold temperature 900 °C) exhibits an average grain size of 2,199 μm, while when the pouring temperature is reduced to 1,480 °C and the mold

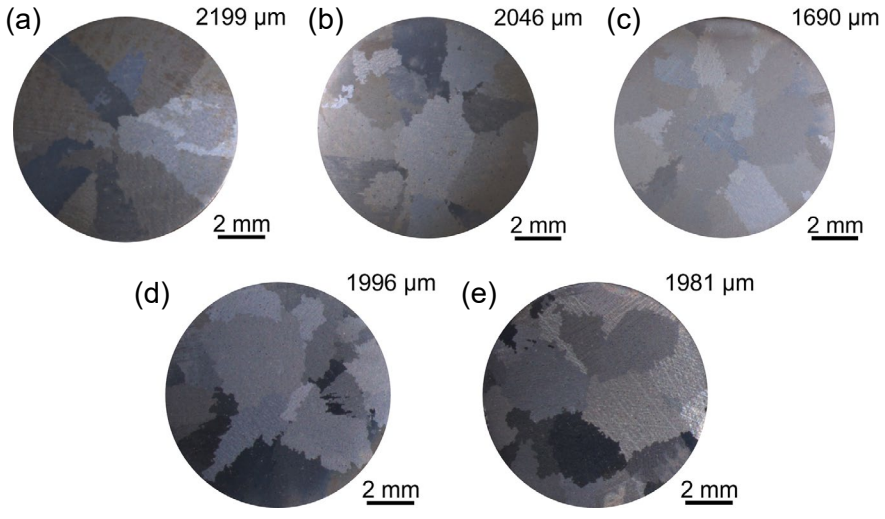


Fig. 2: Grain morphologies and size under different conditions: (a) Sample 1; (b) Sample 2; (c) Sample 3; (d) Sample 4; (e) Sample 5

temperature decreases to 700 °C (Sample 3), the average grain size decreases to 1,690 μm. Under the same pouring temperature (1,480 °C) and mold temperature (900 °C) conditions, different heat treatment processes show minimal impact on grain size, with variations only ranging from 1,981 μm (Sample 5) to 2,046 μm (Sample 2), as illustrated in Fig. 3 and detailed in Table 3.

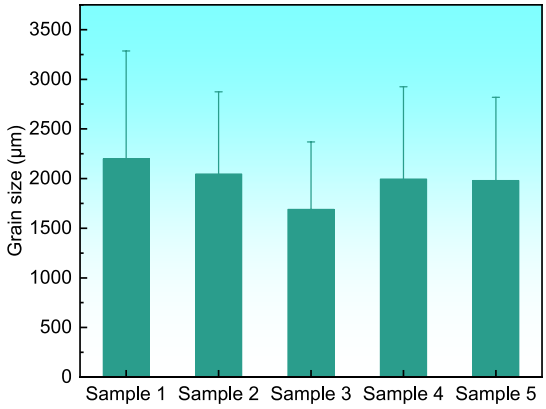


Fig. 3: Grain size under different conditions

3.2.2 MC carbides and (γ+γ') eutectics

Figure 4 shows the morphological characteristics of MC carbides and γ+γ' eutectics under different processing conditions. MC carbides are mainly distributed in blocky and short rod-like morphologies within grains and at grain boundaries, while the blocky γ+γ' eutectics appear at grain boundaries and in interdendritic regions. Sample 3 contains a higher amount of eutectics, which is attributable to the non-equilibrium structure of γ+γ' eutectics. The lower pouring and mold temperatures increase the cooling rate, thereby promoting eutectic precipitation and leading to a higher retained eutectic fraction even after heat treatment. Accordingly, the area fraction of γ+γ' eutectics increases from 1.15% in Sample 1 (pouring temperature 1,520 °C, mold temperature 900 °C) to 2.56% in Sample 2 (1,480 °C/900 °C), and further to 4.99% in Sample 3 (1,480 °C/700 °C).

Table 3: Size of grains and precipitates under different experimental parameters

Sample No.	Grain size (μm)	MC carbide (μm)	(γ+γ') eutectic (μm)	Area fraction (%)	γ' phase size (μm)			
				MC carbides/(γ+γ') eutectics	Dendrite core		Interdendritic region	
					Primary γ'	Secondary γ'	Primary γ'	Secondary γ'
1	2,199±1,086	8.036±2.516	16.02±6.81	2.78±0.10/1.15±0.12	1.288±0.279	0.481±0.070	1.880±0.562	0.476±0.079
2	2,046±829	5.326±2.048	13.81±6.24	3.23±0.11/2.56±0.29	1.167±0.369	0.470±0.064	1.763±0.707	0.468±0.060
3	1,690±679	3.844±1.008	8.60±4.21	1.53±0.05/4.99±1.12	–	0.477±0.082	1.290±0.289	0.462±0.089
4	1,996±928	5.286±1.252	13.27±5.68	2.15±0.14/1.49±1.22	1.188±0.343	0.501±0.093	1.792±0.786	0.498±0.085
5	1,981±838	4.982±1.704	12.47±4.86	1.70±0.10/1.57±0.22	2.399±0.347	0.803±0.161	2.593±0.483	0.744±0.134

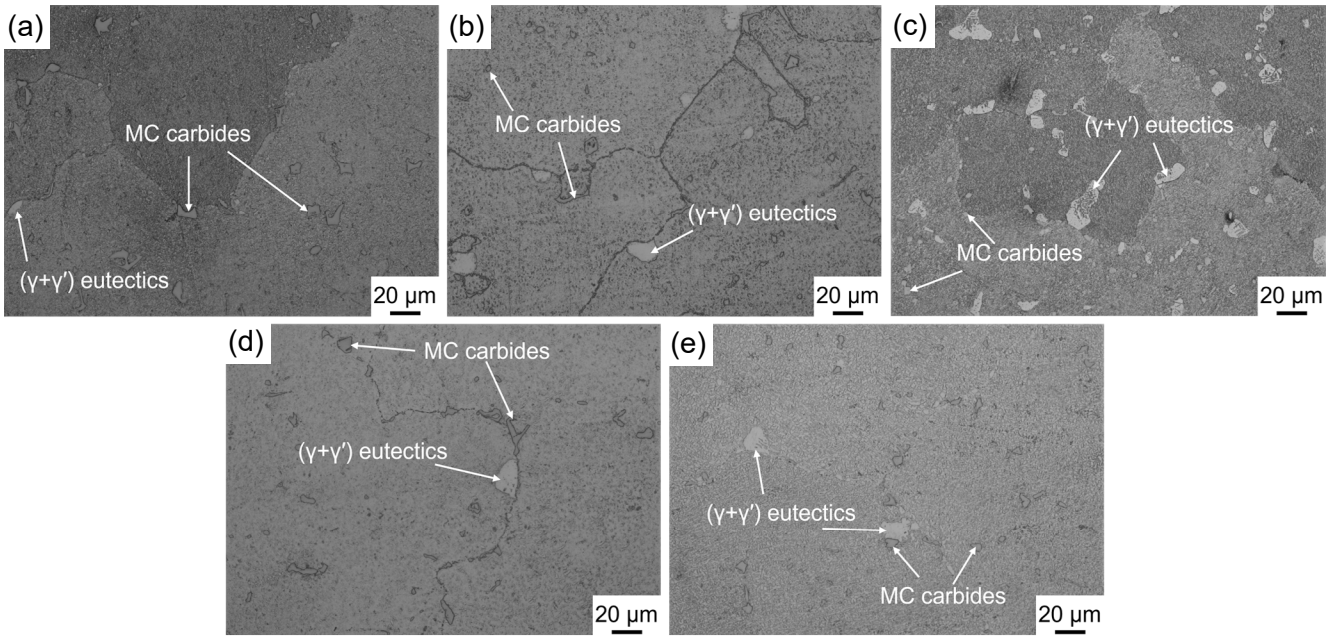


Fig. 4: Morphologies of MC carbides and (γ+γ') eutectics: (a) Sample 1; (b) Sample 2; (c) Sample 3; (d) Sample 4; (e) Sample 5

Meanwhile, the eutectic is refined with decreasing both pouring and mold temperatures, as evidenced by the reduced eutectic size from 16.02 μm (Sample 1) to 13.81 μm (Sample 2) and 8.60 μm (Sample 3). As the pouring and mold temperatures decrease, the average size of MC carbides decreases significantly. The average MC carbide size in Sample 1 is 8.036 μm, whereas that in Sample 3 is only 3.844 μm. Under the same pouring temperature and mold temperature conditions (1,480 °C/900 °C), the average carbide size remains within 4.982–5.326 μm after different heat treatments (Table 3 and Fig. 5), indicating that heat treatment has a relatively limited effect on the average size of carbides.

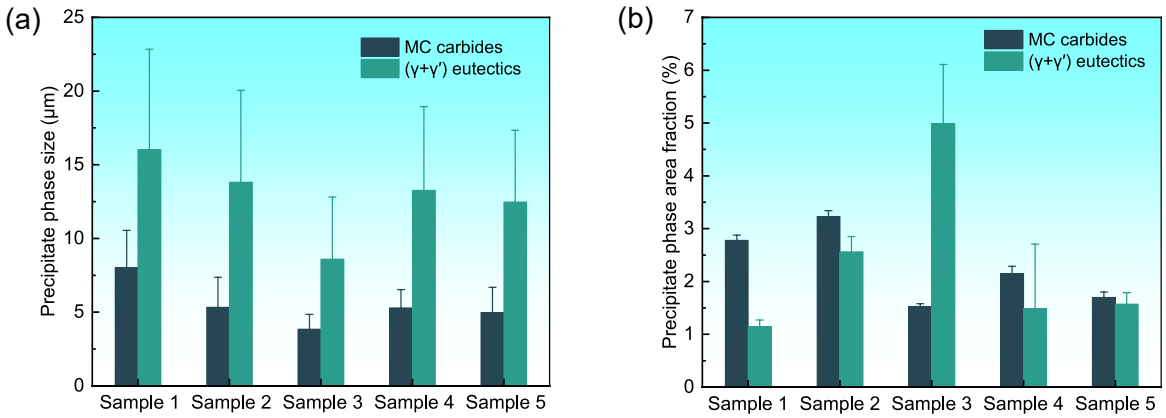


Fig. 5: Size (a) and area fraction (b) of MC carbides and (γ+γ') eutectics under various experimental parameters

3.2.3 γ' phase

Figures 6 and 7 show the morphological characteristics and size distribution of γ' phase in dendritic cores and interdendritic regions under different processing conditions. After solidification under different pouring and mold temperatures, followed by solution heat treatment under various cooling conditions, the γ' phase displays a variety of morphological distributions in the γ matrix, including large and irregular primary γ' phase as well as small secondary γ' phase with a certain degree of cubicity.

Systematic analysis indicates that the primary γ' phase in the interdendritic regions is consistently larger than that in the dendritic cores under all test conditions, which is directly related to the greater elemental segregation in interdendritic regions. Pouring temperature and mold temperature are key process parameters affecting the size of primary γ' phase. As shown in Fig. 7(a), when the pouring temperature decreases from 1,520 °C (Sample 1) to 1,480 °C (Sample 2), even after solution treatment under identical conditions (1,210 °C/240 min+air cooling), the primary γ' phase size decreases from 1.288 μm to 1.167 μm in dendritic cores, and from 1.880 μm to 1.763 μm in interdendritic regions. When the mold temperature is reduced from 900 °C (Sample 2) to 700 °C (Sample 3), under the same pouring temperature (1,480 °C) and solution conditions, no primary γ' phase is detected in the dendritic cores, and the primary γ' phase size in interdendritic regions decreases significantly from 1.763 μm to 1.290 μm. The cooling rate after solution treatment dominates the formation of secondary γ' phase. As shown in Fig. 7(b), the secondary γ' phase sizes in dendritic cores and interdendritic regions under furnace cooling conditions (Sample 4) are 0.501 μm and 0.498 μm, respectively, which are larger than the values of 0.470 μm and 0.468 μm under air cooling (Sample 2). The aging treatment (1,100 °C/120 min) exerts the most significant impact on γ' phase size. Results from Sample 5 show that after aging treatment, the primary γ' phase sizes in dendritic cores and interdendritic regions reach 2.399 μm and 2.593 μm, respectively, considerably larger than those in the non-aged Sample 4 (1.188 μm and 1.792 μm). The secondary γ' phase sizes also increase significantly to 0.803 μm and 0.744 μm. Additionally, ultra-fine γ' phase appears in the γ channels after aging treatment.

3.3 Tensile properties at 1,000 °C

Figure 8 shows the instantaneous tensile properties of all samples at 1,000 °C. In high temperature and high stress environments, the superalloys exhibit an inherent contradiction between strength and ductility. The experimental results indicated that the key process factors affecting the tensile properties are not mold or pouring temperatures, but rather the cooling method after solution heat treatment and subsequent aging treatment. Specifically, when using air cooling (Sample 2), the alloy exhibits higher tensile strength (532.00±10.24 MPa) and yield strength (394.25±3.77 MPa), but significantly lower ductility, including an elongation of (4.00±1.08)%, and a reduction of area of (7.00±2.16)%. In contrast, under furnace cooling (Sample 4) and furnace cooling plus aging treatment (Sample 5) conditions, the elongations increase to (9.75±1.06)% and (11.75±0.35)%, respectively, and the reductions of area improve to (14.00±1.41)% and (17.50±2.12)%, but the tensile strengths correspondingly decrease to 513.5±6.36 MPa and 477.5±7.79 MPa. The results demonstrate that rapid cooling after solution treatment helps maintain the high-temperature strength of the alloy but significantly reduces its ductility, whereas slow (furnace) cooling and aging treatment increase high-temperature ductility while inevitably weakening the strength. Therefore, the cooling route adopted after solution heat treatment is a critical process parameter determining

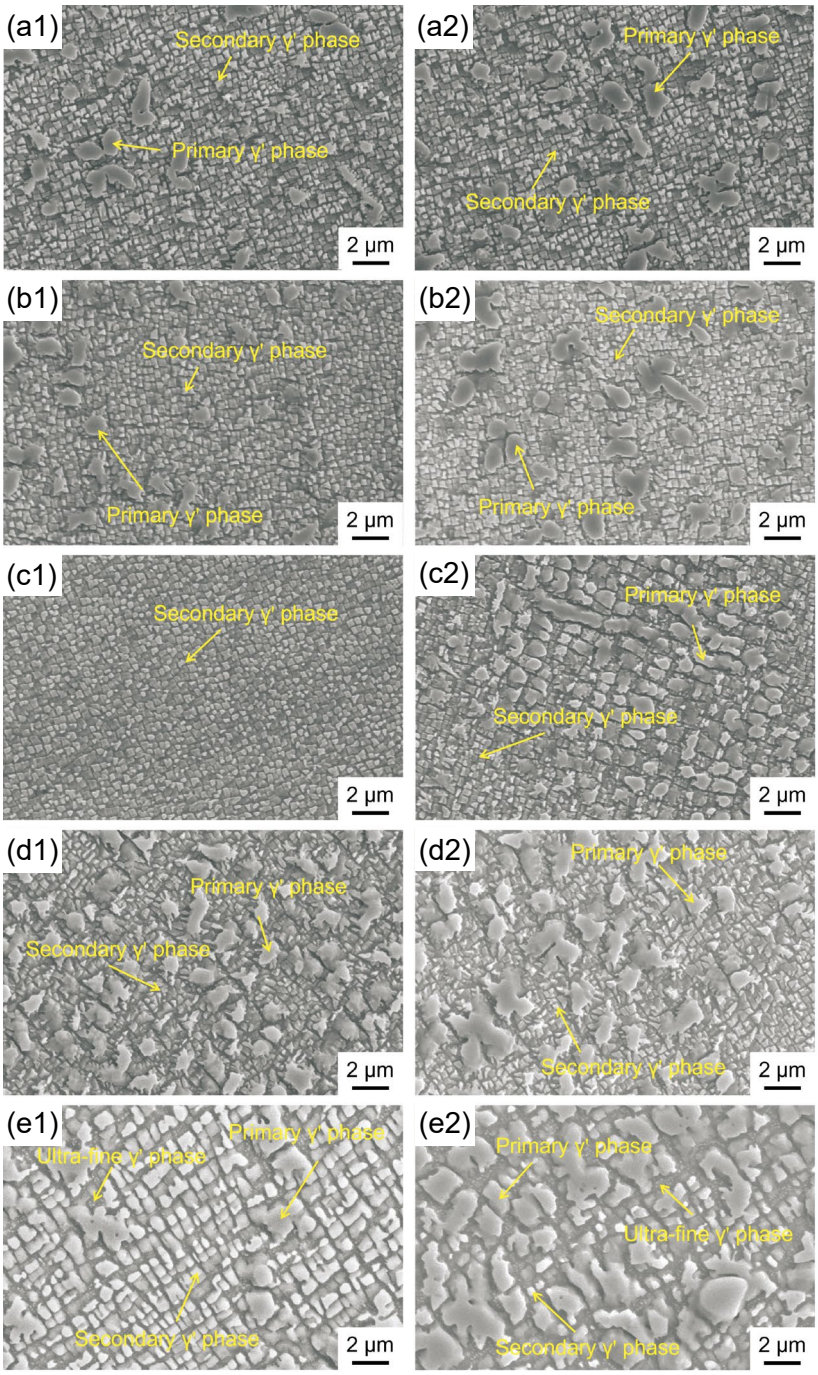


Fig. 6: Morphologies of γ' phase in dendrite cores (a1–e1) and interdendritic regions (a2–e2): (a1, a2) Sample 1; (b1, b2) Sample 2; (c1, c2) Sample 3; (d1, d2) Sample 4; (e1, e2) Sample 5

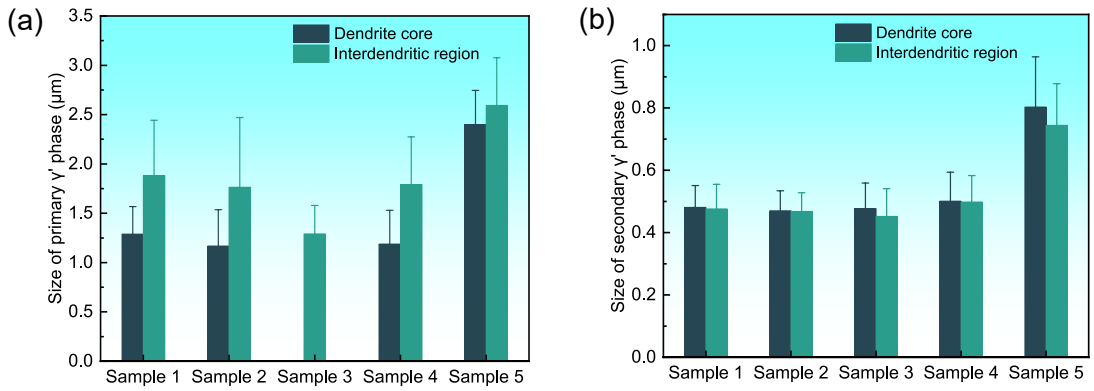


Fig. 7: Size of γ' phase under various experimental parameters: (a) primary γ' phase size; (b) secondary γ' phase size

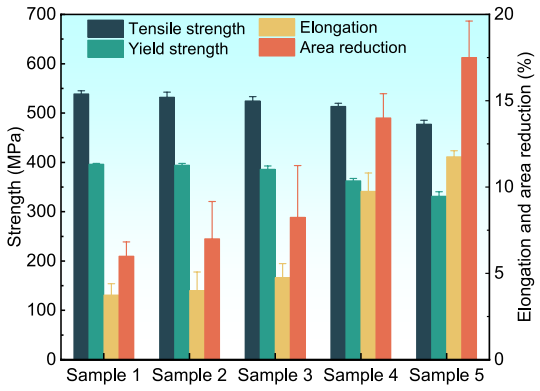


Fig. 8: Tensile properties of superalloy at 1,000 °C under various experimental parameters

the high-temperature mechanical properties of the alloy. In practical process optimization, the high-temperature strength and ductility requirements should be balanced according to specific service conditions, and cooling and subsequent treatment plans should be reasonably formulated to achieve the optimal configuration of high-temperature service performance of the alloy.

3.4 Fracture characteristics

SEM observations of the fracture surfaces after tensile testing at 1,000 °C are shown in Fig. 9. The fracture morphology exhibits mixed intergranular and ductile fracture characteristics. Numerous dimples are observed on the fracture surfaces of Samples 4 and 5 with higher elongations, showing

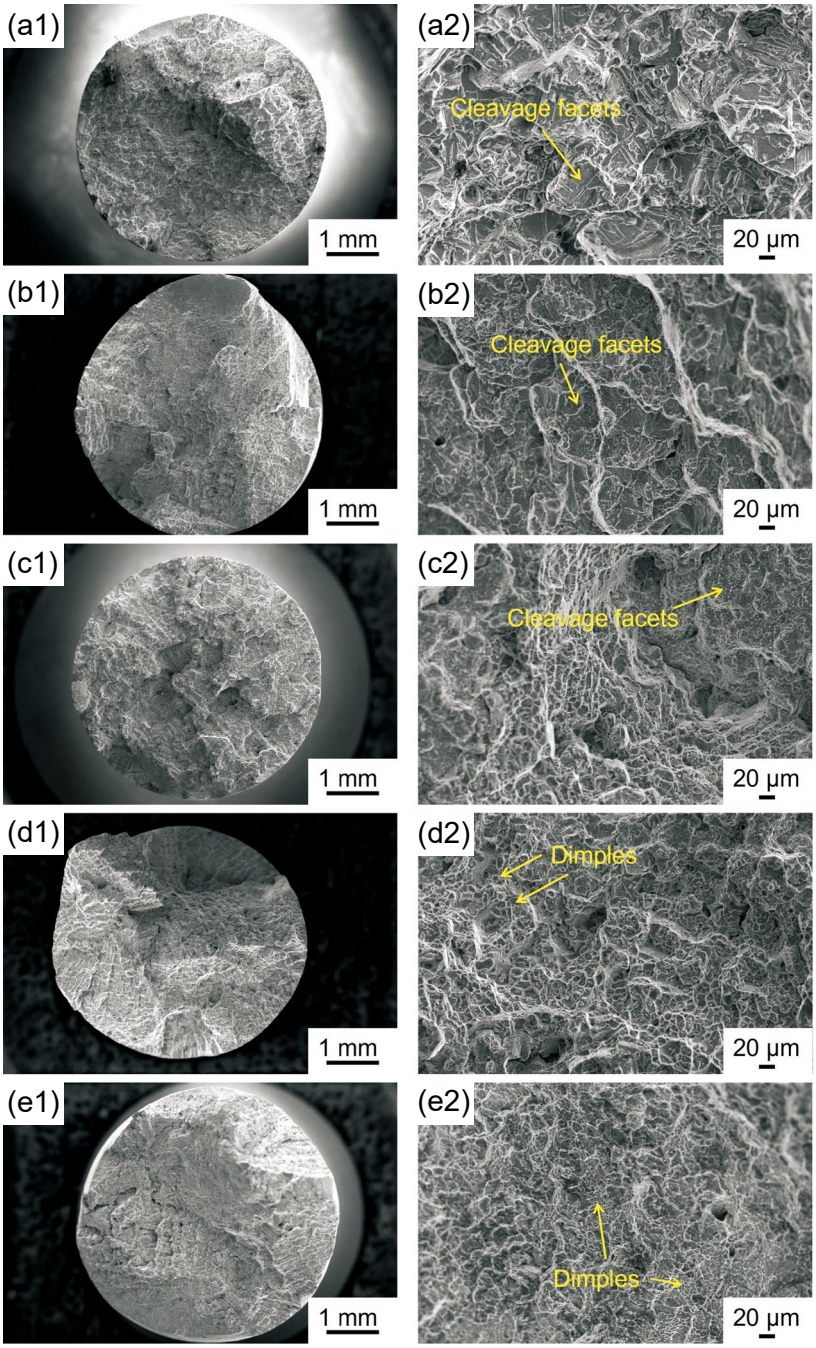


Fig. 9: Microstructure characteristics of fracture surface after tensile testing at 1,000 °C: (a1, a2) Sample 1; (b1, b2) Sample 2; (c1, c2) Sample 3; (d1, d2) Sample 4; (e1, e2) Sample 5

significant ductile fracture features. In contrast, intergranular fracture characteristics dominate in Samples 1 to 3 with lower elongations, which contain more cleavage facets. Figure 10 shows the longitudinal section near the fracture surface and the crack propagation path. At a high temperature of 1,000 °C, cracks mainly propagate along grain boundaries and interdendritic regions. Microscopic observation indicates that cracks first form around MC carbides and then extend along grain boundaries. This phenomenon suggests that MC carbides at grain boundaries easily induce stress concentration and act as microcrack initiation sites. Under the combined effect of high temperature and high stress, sliding and deformation occur at MC carbide/matrix and eutectic/matrix interfaces, forming preferential regions for microcrack initiation. Once microcracks form, they propagate along grain boundaries and interdendritic regions, eventually leading to material failure. The observed crack characteristics are highly consistent with the results reported by Zhai et al[15].

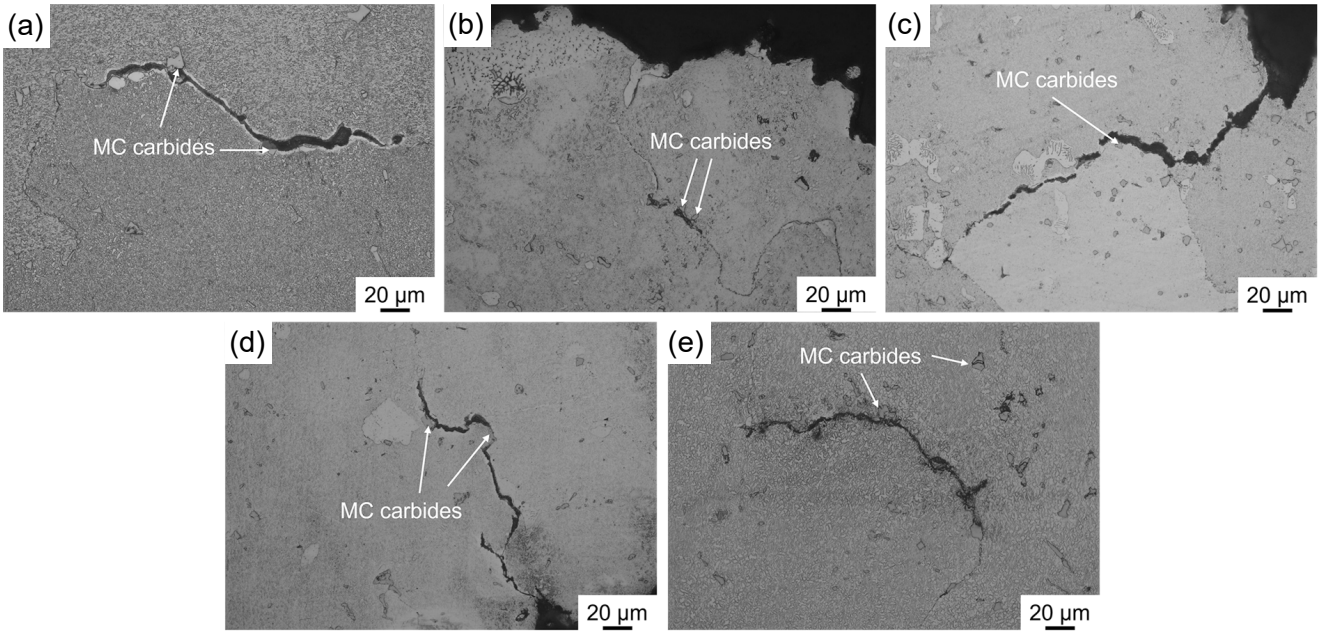


Fig. 10: Microstructure characteristics of longitudinal section near the fracture after tensile testing at 1,000 °C: (a) Sample 1; (b) Sample 2; (c) Sample 3; (d) Sample 4; (e) Sample 5

4 Discussion

4.1 Effect of process parameters on microstructure

Results in this study indicate that pouring temperature, mold temperature, cooling rate after solution treatment, and aging treatment show varying degrees of influence on the grain size, MC carbide size, and γ' phase size in both interdendritic regions and dendritic cores of the superalloy. According to classical nucleation theory, the critical nucleation size, corresponding critical nucleation energy, and nucleation rate can be expressed as follows[15]:

$$r^* = \frac{2\sigma T_m}{\Delta H_V \Delta T} \tag{1}$$

$$\Delta G^* = \frac{16\pi\sigma^3 T_m^2}{3\Delta H_V^2 \Delta T^2} \tag{2}$$

$$I = K \cdot e^{-\Delta G^*/kT} \cdot e^{-Q/kT} \tag{3}$$

where r^* is the critical nucleation radius, m; σ is the liquid-solid interface energy per unit area, J·m^{-2}; T_m is the melting temperature of metal, K; ΔH_V is the melting enthalpy per unit volume of melt, J·m^{-3}; ΔT is nucleation undercooling, K; ΔG^* is the critical nucleation work, J·m^{-3}; K is the proportional constant, s^{-1}·m^{-3}; I is the nucleation rate, s^{-1}·m^{-3}; k is Boltzmann constant; T is nucleation temperature, K; and Q is the diffusion activation energy of metal atoms through the solid-liquid interface, J·m^{-3}.

Mueller et al.[16] demonstrated that nucleation undercooling is closely related to the cooling rate during melt solidification, showing a monotonic increase with higher cooling rates until eventually approaching a specific limiting value. In this study, reducing the pouring temperature and mold temperature effectively increases the melt cooling rate, thereby enhancing nucleation undercooling. According to Eqs. (1)–(3), increased nucleation undercooling results in smaller critical nucleation size and reduced critical nucleation energy, while significantly increasing the nucleation rate, ultimately leading to refined grain and MC carbide. Additionally, faster cooling rates also delay the growth of grains and MC carbides to some extent, promoting microstructural refinement.

Primary γ' phases form during melt solidification, with their size negatively correlates with nucleation undercooling[8]. As pouring temperature and mold temperature decrease, increased cooling rates promote higher nucleation undercooling in as-cast primary γ' phases, thereby reducing their size. After solution heat treatment under identical conditions, the corresponding residual primary γ' phase size decreases accordingly. In this study, at the mold temperature of 700 °C, no residual primary

γ' phases are found in the dendritic cores of the solution-treated and air-cooled sample (Sample 3), possibly because the initial small as-cast γ' phases in this region completely dissolved into the γ matrix during the solution heat treatment process. Although the overall size of primary γ' phases under different process parameters is influenced by nucleation undercooling, under the same undercooling conditions, the residual primary γ' phase size in interdendritic regions is significantly larger than in dendritic cores. This occurs because γ' phase-forming elements Al and Ti have higher concentrations in interdendritic regions[7, 8, 14], creating greater compositional supersaturation that promotes preferential nucleation of as-cast primary γ' phases in these areas. Consequently, γ' phases in interdendritic regions are larger, and this size difference persists after heat treatment.

During the solution heat treatment process, as-cast primary γ' phases dissolve into the γ matrix, and subsequently reprecipitate as smaller, somewhat cuboidal secondary γ' phases during the cooling process. Higher cooling rates lead to greater nucleation undercooling of secondary γ' phases, correspondingly increasing the nucleation rate. Therefore, secondary γ' phases formed under air-cooling conditions (Sample 2) are smaller in size than those formed under furnace-cooling conditions (Sample 4).

Experimental and theoretical studies have shown that γ' precipitate phases in nickel-based alloys inevitably undergo coarsening during prolonged high-temperature exposure, This morphological evolution is driven by the equilibrium adjustment between interfacial energy and elastic energy[17-19]. This mechanism explains the fundamental origin of γ' phase coarsening observed in the aged sample (Sample 5). Additionally, during the high-temperature aging process, γ'-forming elements diffuse from the γ' precipitates to the γ matrix[20], resulting in elemental supersaturation in the γ matrix. During the subsequent cooling process, numerous ultrafine γ' particles reprecipitate from the supersaturated γ matrix, as shown in Figs. 6(e1) and (e2).

4.2 Effect of microstructure on mechanical properties

It is well known that grain size and distribution of γ' phase sizes in different regions significantly influence the mechanical properties of cast polycrystalline superalloys[21-23]. Among these factors, the effect of grain size on alloy performance has long been a research focus in the field of materials science. As early as the 1950s, Hall and Petch[24, 25] proposed the famous Hall-Petch relationship during their investigations on low-carbon steels, illustrating the quantitative correlation between grain size and yield strength:

$$\sigma = \sigma_0 + k_d d^{-1/2} \quad (4)$$

where σ is the yield strength of the metallic material; σ_0 is the frictional resistance of the grain against dislocation movement; k_d is the level of stress concentration at the grain boundary caused by dislocation accumulation, which correlates with the number of effective slip systems; d is the grain diameter.

In this study, a Pearson correlation matrix is computed to systematically evaluate the relationships between microstructural parameters and mechanical properties, as visualized in the heatmap (Fig. 11). The analysis reveal a weak positive correlation between strength and grain size (r=0.19), with slightly increased strength corresponding to larger grain sizes. This observation runs contrary to the conventional Hall-Petch relationship, suggesting that precipitation strengthening (γ' phases, r>0.88) dominates over grain boundary strengthening in this alloy system. Previous research has established that polycrystalline alloys demonstrate substantially different mechanical behaviors across various temperature regimes[26]. During creep processes, the influence of grain size on the tensile strength of nickel-based polycrystalline alloys fundamentally differs between intermediate temperature (700 °C to 900 °C) and high temperature (above 900 °C) conditions[6]. Research by Du et al.[27] demonstrated that at 760 °C, cracks predominantly propagate in a transgranular mode, indicating that grain boundary strength exceeds intragranular strength at this temperature, with plastic deformation primarily occurring through activation of intragranular slip systems. Consequently, smaller grain sizes result in shorter slip band lengths, promoting more uniform intragranular deformation and facilitating coordinated deformation between grains, thereby enhancing creep resistance[28]. In contrast, under 950 °C creep conditions, cracks exhibit intergranular fracture patterns with plastic deformation concentrated at grain boundaries, indicating significant grain boundary sliding phenomena[6]. The tensile fracture mode observed in this study at 1,000 °C similarly displays intergranular fracture characteristics, consistent with the aforementioned high-temperature research findings.

Deformation in metallic materials primarily occurs through slip mechanisms, with dislocation theory providing a fundamental framework for understanding variations in mechanical properties. In nickel-based superalloys, precipitated γ' phases effectively impede dislocation movement, thereby significantly enhancing alloy strength. For this reason, γ' phases are widely recognized as the critical strengthening phase in nickel-based superalloys, with their morphology and distribution directly determining the mechanical properties of these superalloys in high-temperature environments[29-31]. This study revealed a clear correlation between tensile properties and γ' phase size under high-temperature conditions of 1,000 °C. Experimental results demonstrate that the sizes of both primary and secondary γ' phases, whether in interdendritic regions or dendritic cores, exhibit a pronounced negative correlation with tensile strength and yield strength. As the size of γ' phases increases, alloy strength progressively decreases with diminished strengthening effects, while elongation correspondingly increases. This phenomenon can be reasonably explained through the microscopic mechanisms of interaction between γ' phases and dislocations.

The γ' phases impede dislocation movement through two primary mechanisms: the shearing mechanism, where

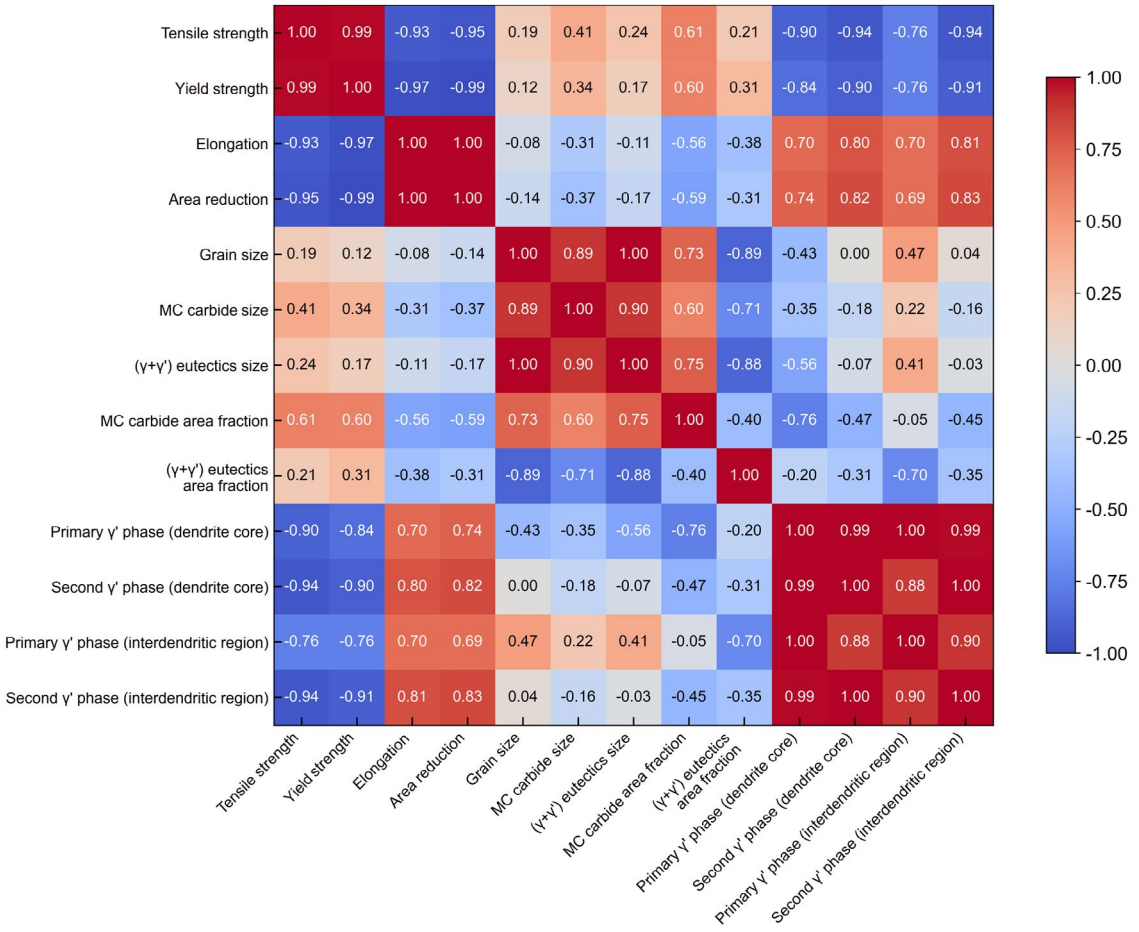


Fig. 11: Correlation between tensile properties at 1,000 °C and microstructure of superalloy

dislocations cut through γ' phases, and the Orowan mechanism, where dislocations bypass γ' phases[10]. While dislocations tend to cut through precipitates when γ' phases are relatively small, the stress required for dislocation bypassing gradually decreases as γ' phase size increases, causing the dislocation movement mechanism to transition from shearing to bypassing once this critical value falls below the stress needed for cutting, at which point the Orowan mechanism becomes dominant and the strengthening effect subsequently diminishes[12, 32]. The phenomena observed in this study demonstrate strong consistency with this theoretical model and other research findings[10, 11, 33, 34], specifically that increased γ' phase size leads to diminished strengthening effects, ultimately manifested as a reduction in alloy strength.

5 Conclusions

This study systematically investigated the effects of pouring and mold temperatures, and heat treatment parameters on the microstructure and high-temperature mechanical properties of nickel-based polycrystalline superalloys, as well as the relationship between microstructural features and tensile properties at 1,000 °C. The main conclusions are as follows:

(1) Reducing both pouring and shell mold temperatures effectively decreases grain size and MC carbide dimensions. Furthermore, lower pouring and mold temperatures promote refinement of as-cast primary γ' phases, subsequently reducing the size of residual primary γ' phases after heat treatment.

(2) The cooling route following solution heat treatment significantly influences the high-temperature mechanical properties of the alloy. The alloy subjected to air cooling demonstrates higher tensile strength (532.00±10.24 MPa) but lower ductility, with an elongation of (4.00±1.08)%. In contrast, furnace cooling followed by aging treatment substantially enhances high-temperature ductility, yielding a maximum elongation of (11.75±0.35)%, while the tensile strength decreases correspondingly to 477.5±7.79 MPa.

(3) At 1,000 °C, a clear correlation exists between γ' phase size and mechanical properties. As the sizes of γ' phases increase, both tensile strength and yield strength of the alloy progressively decrease, while elongation correspondingly increases, indicating that the size of γ' phase constitutes a critical microstructural factor influencing high-temperature mechanical properties.

(4) High-temperature (1,000 °C) tensile fracture analysis reveals predominantly intergranular fracture characteristics. Cracks primarily propagate along grain boundaries and interdendritic regions. Experimental observations show that cracks initially nucleate around MC carbides and subsequently extend along grain boundaries, confirming that MC carbides located at grain boundaries serve as stress concentration sites and microcrack initiation origins at high temperatures.

Conflict of interest

The authors declare that they have no known competing financial interests or personal relationships that could have appeared to influence the work reported in this paper.

References

[1] Hardy M C, Detrois M, McDevitt E T, et al. Solving recent challenges for wrought Ni-base superalloys. Metallurgical and Materials Transactions: A, 2020, 51(6): 2626–2650.
[2] Wu Y T, Li C, Li Y F, et al. Effects of heat treatment on the microstructure and mechanical properties of Ni_3Al-based superalloys: A review. International Journal of Minerals, Metallurgy and Materials, 2021, 28(4): 553–566.
[3] Giridhar G and Pandey A K. Recent developments in nickel-based superalloys for gas turbine applications: Review. Journal of Alloys and Compounds, 2023, 963.
[4] Pollock T M and Tin S. Nickel-based superalloys for advanced turbine engines: Chemistry, microstructure and properties. Journal of Propulsion and Power, 2006, 22(2): 361–374.
[5] Zhang J, Jie Z Q, Huang T W, et al. Research and development of equiaxed grain solidification and forming technology for nickel-based cast superalloys. Acta Metallurgica Sinica, 2019, 55(9): 1145–1159.
[6] Zhang C J, Wang P, Wen Z X, et al. Study on creep properties of nickel-based superalloy blades based on microstructure characteristics. Journal of Alloys and Compounds, 2021, https://doi.org/10.1016/j.jallcom.2021.161710.
[7] Jie Z Q, Zhang J, Huang T W, et al. The influence of melt superheating treatment on the cast structure and stress rupture property of IN718C superalloy. Journal of Alloys and Compounds, 2017, 706: 76–81.
[8] Cui H Y, Tan Y, Bai R S, et al. Effect of melt superheat treatment on solidification behavior and microstructure of new Ni-Co based superalloy. Journal of Materials Research and Technology, 2021, 15: 4970–4980.
[9] Wang C, Sheng N, Sun S, et al. Addition of nitrogen in Ni-based cast superalloys: Microstructures and properties. Materials Science and Engineering: A, 2025, 944: 148907.
[10] Wang W Z, Hong H U, Kim I S, et al. Influence of γ′ and grain boundary carbide on tensile fracture behaviors of Nimonic 263. Materials Science and Engineering: A, 2009, 523(1–2): 242–245.
[11] Joseph C, Persson C, and Hörnqvist C M. Influence of heat treatment on the microstructure and tensile properties of Ni-base superalloy Haynes 282. Materials Science and Engineering: A, 2017, 679: 520–530.
[12] Valle J A D, Picasso A C, and Romero R. Work-hardening in Inconel X-750: Study of Stage II. Acta Materialia, 1998, 46(6): 1981–1988.
[13] Academic Committee of the Superalloys C. China superalloys handbook. Beijing: Standards Press of China, 2012: 168–176. (In Chinese)
[14] Jing G Y, Li A Q, Sun X, et al. Effect of melt superheating on solidification microstructure and mechanical properties of K424 superalloy. China Foundry, 2025, 22(3): 252–262.
[15] Zhai Q J. Foundamentals of structure refinement technology for metal solidification. Beijing: Science Press, 2018: 26–27. (In Chinese)
[16] Mueller B A and Perepezko J H. The undercooling of aluminum. Metallurgical Transactions: A, 1987, 18A: 1143–1150.
[17] Tiley J, Viswanathan G B, Srinivasan R, et al. Coarsening kinetics of γ′ precipitates in the commercial nickel base superalloy René 88 DT. Acta Materialia, 2009, 57(8): 2538–2549.
[18] Zhang P, Yuan Y, Yan J B, et al. Morphological evolution of γ′ precipitates in superalloy M4706 during thermal aging. Materials Letters, 2018, 211: 107–109.
[19] Lapin J and Vaňo A. Coarsening kinetics of α- and γ′-precipitates in a multiphase intermetallic Ni-Al-Cr-Ti type alloy with additions of Mo and Zr. Scripta Materialia, 2004, 50(5): 571–575.
[20] Tong J Y, Feng W, Fu C, et al. Microstructural degradation and mechanical properties of GH4033 alloy after overheating for short time. Acta Metallurgica Sinica, 2015, 51(10): 1242–1252.
[21] Yuan X F, Song J X, Zheng Y R, et al. Quantitative microstructural evolution and corresponding stress rupture property of K465 superalloy. Materials Science and Engineering: A, 2016, 651: 734–744.
[22] Torster F, Baumeister G, Albrecht J, et al. Influence of grain size and heat treatment on the microstructure and mechanical properties of the nickel-base superalloy U720LI. Materials Science and Engineering: A, 1997, A234–236: 189–192.
[23] Yuan X F, Song J X, Zheng Y R, et al. Abnormal stress rupture property in K465 superalloy caused by microstructural degradation at 975 °C/225 MPa. Journal of Alloys and Compounds, 2016, 662: 583–592.
[24] Hall E O. The Deformation and ageing of mild steel. In: Proceedings of the Physical Society, 1951, B64: 747–753.
[25] Petch N J. The cleavage strength of polycrystals. Journal of the Iron and Steel Institute, 1953, 174: 25.
[26] Shingledecker J P, Evans N D, and Pharr G M. Influences of composition and grain size on creep-rupture behavior of Inconel® alloy 740. Materials Science and Engineering: A, 2013, 578: 277–286.
[27] Du B N, Yang J, X, Cui C Y, et al. Effects of grain refinement on creep properties of K417G superalloy. Acta Metallurgica Sinica, 2014, 50(11): 1384–1392.
[28] Soula A, Renollet Y, Boivin D, et al. Analysis of high-temperature creep deformation in a polycrystalline nickel-base superalloy. Materials Science and Engineering: A, 2009, 510–511: 301–306.
[29] Wang S A, Wang L, Liu Y, et al. Effect of long-term aging on the fatigue crack growth rate of a nickel-based superalloy. Materials Science and Engineering: A, 2011, 528(4/5): 2110–2117.
[30] Murakumo T, Kobayashi T, Koizumi Y, et al. Creep behaviour of Ni-base single-crystal superalloys with various γ′ volume fraction. Acta Materialia, 2004, 52(12): 3737–3744.
[31] Van Sluytman J S and Pollock T M. Optimal precipitate shapes in nickel-base γ-γ′ alloys. Acta Materialia, 2012, 60(4): 1771–1783.
[32] Oh J H, Choi I C, Kim Y J, et al. Variations in overall- and phase-hardness of a new Ni-based superalloy during isothermal aging. Materials Science and Engineering: A, 2011, 528(19–20): 6121–6127.
[33] Gayda J and Miner R V. The effect of microstructure on 650 °C fatigue crack growth in P/M astroloy. Metallurgical Transactions: A, 1983, 14: 2301–2308.
[34] Shin K Y, Kim J H, Mathieu T, et al. Effects of heat treatment on the microstructure evolution and the high-temperature tensile properties of Haynes 282 superalloy. Materials Science and Engineering: A, 2019, 751: 311–322.